Label-Free *in situ* Raman Analysis of Opposite and Tension Wood in *Populus nigra*

Jianfeng Ma, Xia Zhou, Xun Zhang, and Feng Xu*

Label-free *in situ* confocal Raman microscopy has been used to investigate the differences in cell morphology and components distribution between opposite wood (OW) and tension wood (TW) in *Populus nigra*. In the Raman images showing the ratio of the 1657 cm^{-1} to the 1603 cm^{-1} band, the spatial heterogeneity in coniferyl alcohol and coniferyl aldehyde (Lignin-CAA) was visualized within both samples. Enrichment of Lignin-CAA was visualized in the CC and CML regions where there was the highest lignin concentration. In fiber S2, which had the highest content of cellulose, there was apparent deficiency in the Lignin-CAA concentration. Raman spectra analysis revealed that the band at 1097.0 cm^{-1} in OW fiber S2 shifted to lower wavenumbers in TW fiber S2 (1094.4 cm^{-1}) and GL (1094.0 cm^{-1}), which resulted from the stretch of the glycosidic C-O-C bond of the cellulose molecular. The negative band shift at 1097 cm^{-1} indicated that the microfibrils in the TW fiber S2 and GL were stretched during TW formation and the microfibrils still kept the tensional deformation even after the fibers were transversally cut. The sub-cellular localization of cellulose and lignin together with the variation in molecular deformation will contribute to understanding the morphological and chemical properties of TW as a desirable woody biomass, as well as the development of its high tensile strength.

Keywords: Opposite and tension wood; Cellulose; Lignin; Molecular deformation; Confocal Raman microscopy

*Contact information: Beijing Key Laboratory of Lignocellulosic Chemistry, Beijing Forestry University, Beijing, China, 100083; *Corresponding author: xfx315@bjfu.edu.cn*

INTRODUCTION

High worldwide demand for energy has led to a resurgence in the exploration for alternative energy that can reduce dependence on fossil fuels (Ragauskas *et al.* 2006). To avoid competition with the food/feed supply, second generation biofuels produced from lignocellulosic biomass have become the focus of significant efforts worldwide (Tilman *et al.* 2006), as it is abundant in nature, renewable, and can be economically obtained (Gomez *et al.* 2008). The conversion process of lignocellulosic biomass typically consists of three steps: pretreatment; hydrolysis of cellulose and hemicelluloses into fermentable sugars; and fermentation of the sugars into liquid fuels and other commodity chemicals. However, biomass recalcitrance currently poses a major impediment for their use in the production of transportation fuels and chemicals. Natural factors believed to contribute to the recalcitrance of lignocellulosic feedstocks to chemicals or enzymes mainly include complex cell wall macromolecular organization and the degree of lignification (Iiyama *et al.* 1994; Himmel *et al.* 2007). In biomass conversion for biofuels, lignin inhibits saccharification in processes aimed at producing simple sugars for fermentation to ethanol. The effective use of plants for industrial purposes is in fact largely dependent on the extent to which the plant cell wall is lignified (Ralph *et al.* 2007). Tension wood (TW) with specialized morphological and chemical properties might be a desirable lignocellulosic substrate for biomass conversion.

TW is a woody biomass that is formed in the upper side of leaning trunks and branches in hardwood species in response to mechanical stress such as wind and gravity. Due to the development of the gelatinous layer (GL), TW exhibits important changes of cell morphological structure and chemical composition, both of which influence the tree mechanics as well as wood properties. The GL has been variously described as filling the cell lumen, as being attached to the S3 layer (S1+S2+S3+GL), as replacing the S3-layer (S1+S2+GL), or partly or entirely substituteing the S2 layer (S1+GL) (Dadwell and Wardrop 1955).

Additionally, TW is characterized by relatively higher cellulose content, a lower degree of lignification, increased number of xylem fibers, and more secondary wall components (biomass), all of which contribute to desirable features of lignocellulosic substrate for bioethanol production (Pilate *et al.* 2004; Foston *et al.* 2011). It has been shown that the relative abundance of lignin subunits (*p*-hydroxyphenyl, guaiacyl, and syringyl units) have great implications for potential bioengineering strategies to improve fermentable sugar release in biofuel production (Siqueira *et al.* 2011; Zhang *et al.* 2012). Specifically, transgenic poplar trees with higher S/G ratios show greatly enhanced biorefining efficiency (Huntley *et al.* 2003). By using time-of-flight secondary ion mass spectrometry, Zhou *et al.* (2011) found that the guaiacyl lignin is predominantly located in the vessel cell walls of poplar wood while syringyl lignin is mainly located in the fiber cell walls. The G/S ratio in vessel cell walls was determined to be approximately twice that found in fiber cell walls. As the immediate precursor for G lignin, the distribution of coniferyl alcohol and coniferaldehyde (Lignin-CAA) in *Picea abies* and *Pinus sylvestris* as well as wild type and lignin-reduced transgenic *Populus trichocarpa* were investigated by Raman imaging (Schmidt *et al.* 2009; Hänninen *et al.* 2011). However, the distribution pattern of Lignin-CAA in poplar TW was scarcely investigated.

Although it has been well established that the GL with its microfibril angle parallel or nearly parallel to the longitudinal axis is the driving force of the tensile stress generated in TW (Fujita *et al.* 1974; Goswami *et al.* 2008), the underlying mechanism at the origin of tensional stress in TW has been the subject of controversy. Different hypotheses have been proposed to explain the mechanism, such as the contraction of amorphous zones within the cellulose microfibrils (Yamamoto 2004), the action of xyloglucans during the formation of microfibril aggregates (Nishikubo *et al.* 2007), or the effect of changes in moisture content stimulated by pectin-like substances (Bowling and Vaughn 2008). However, no literature was found in which an attempt was made to reveal the mechanism at the origin of tensile stress in TW by using in situ vibrational spectroscopy at the sub-cellular level.

Vibrational microscopic analysis, such as Raman and infrared imaging approaches, can provide morphological and molecular structure information of plant cell wall *in situ* with a high spatial resolution. Inelastic Raman scattering depends on changes in the polarisability of vibrating functional groups, while infrared absorption depends on changes of dipole moments (Gierlinger and Schwanninger 2007). However, the infrared imaging is limited by low sensitivity due to non-background-free detection, low spatial resolution associated with the long infrared wavelengths, and water absorption of the infrared light (Evans and Xie 2008). None of these disadvantages exist in Raman imaging, and both lignin and cellulose are Raman active and can be mapped simultaneously. Although auto-fluorescence from phenolic compounds may sometimes interfere with Raman measurement, the addition of D_2O and selection of suitable excitation wavelength can alleviate this problem generally. Raman spectroscopy has also been conducted on polymeric fibres (Davies *et al.* 2004) as well as various forms of cellulose and wood (Kong and Eichhorn 2005; Sturcova *et al.* 2005) to monitor changes during deformation on the molecular level. The method relies on the fact that Raman bands corresponding to the vibrations of

structural groups within polymer chain molecules shift towards a lower wavenumber upon tensile deformation of the polymer material (Batchelder and Bloor 1979).

In the present study, label-free *in situ* confocal Raman microscopy was used to investigate the morphological properties and lignocellulosic chemistry in *Populus nigra* OW and TW, especially differences in cellulose and lignin localization in the cell walls. Furthermore, the molecular deformation variations in cell wall layers were reflected by Raman band shift.

EXPERIMENTAL

Materials

An inclined 10-year-old *P. nigra* tree, provided by the arboretum of Northwest Agricultural and Forestry University, China, was chosen, and wood samples were extracted from both sides of the trunk: OW on the lower side and TW on the upper side. Wood disc was collected at a height of 1.5 m above ground level. Small sample blocks of approximately 15 mm (longitudinal) × 5 mm (tangential) × 10 mm (radial) were cut out from the seventh annual ring of the stem. Without any embedding routine, 20-μm-thick cross-sections for chemical imaging were cut on a sliding microtome (Leica 2010R). In order to avoid the border effect, great care was taken to enhance the quality of the sections. Compression forces due to the penetration of the blade were minimized by using new, perfectly sharp blades (Thermo MX35 Ultra) and appropriate leading angles (45°). Moreover, the sectioning speed must be uniform and fast. In order to avoid the shrinkage due to drying effects the surface of block was covered with a drop of water. For chemical imaging, samples were placed on a glass slide with a drop of D_2O, covered by a coverslip (0.17 mm thickness), and sealed with nail-polish to prevent evaporation during measurement. Immersion in D_2O limited laser-induced fluorescence, and the D-O stretching vibration (2500 cm^{-1}) provided a convenient external reference for Raman intensity measurements (Agarwal and Atalla 1986).

Confocal Raman Microscopy

Raman spectra were acquired with a LabRam Xplora confocal Raman microscope (Horiba Jobin Yvon) equipped with a confocal microscope (Olympus BX51) and a motorized x, y stage. In order to achieve high spatial resolution, measurements were conducted with a high numerical aperture (NA) microscope objective from Olympus (100×, oil, NA=1.40), and a linear-polarized 532-nm laser excitation was focused with a diffraction-limited spot size (theoretically $1.22\lambda/NA$). The laser power on the sample was approximately 8 mW. The Raman light was detected by an air-cooled, front-illuminated spectroscopic charge-coupled device (CCD) behind a grating (2400 grooves mm^{-1}) spectrometer with a spectral resolution of 1.5 cm^{-1}. For mapping, 0.5 μm steps were chosen and every pixel corresponds to one scan. The spectrum from each location was obtained by averaging 4-s cycles. Confocal aperture was set at 100 μm for all experiments. The reported depth resolution for the 400 μm confocal hole, based on the silicon (standard) phonon band at 520 cm^{-1}, was 2 μm. The lateral resolution of the confocal Raman microscope in our study was significantly lower than the theoretical prediction ($0.61\lambda/NA \approx 231$ nm). Different chemical images were generated by means of a cosmic ray removal filter, and then sum filters of the software (Labspec) were applied for integrating defined regions in the wood spectra. Within the chosen areas, the sum filter calculated the intensities. Within the chemical images, defined areas of interest could be marked and average spectra were calculated for a

detailed analysis. Moreover, the cell wall thickness was measured according to the Raman images using the AxioVision Rel. 4.7 software from 10 cells.

Data Processing

For samples used in this study, semi-quantitative determinations require a normalization procedure. Prior to accurate normalization, the spectral background subtraction was performed by taking the baseline from the first to the second border. A multi-point linear baseline was subtracted from each Raman spectrum. Baseline points were set at minima near 700 cm^{-1}, 1500 cm^{-1}, 1800 cm^{-1}, 2100 cm^{-1}, 2800 cm^{-1}, and 3000 cm^{-1}. To determine the Raman peak height and position of morphologically distinct areas, the resulting spectra were deconvoluted at 1587 cm^{-1}, 1603 cm^{-1}, 1622 cm^{-1}, 1657 cm^{-1}, and 1683 cm^{-1} (Fig. 1 inset). The deconvolution of the spectra by peak fitting was performed using Gauss-lorenz mixture function. The measured peak height was converted to the corresponding relative intensity by dividing it by the D_2O band intensity at 2500 cm^{-1} ($I_{1603\ cm^{-1}}/I_{2500\ cm^{-1}}$ and $I_{1657\ cm^{-1}}/I_{2500\ cm^{-1}}$). Relative intensity and standard deviation were calculated from three different set of spectra, deconvoluted one at a time. The three different set of spectra were extracted separately from the three different CC and S2 of three single cells in Fig. 2a and 2b.

RESULTS AND DISCUSSION

Raman microspectroscopy provides a spatial distribution of intact plant cell wall components in their native form. Detailed spatial insights into the composition of the cell wall are critical to better understand the chemical, biological, and mechanical properties of lignocellulosic biomass. The average Raman spectra extracted from various layers of OW and TW fiber, recorded from 70×70 μm^2 sample areas of cross-sections in D_2O and normalized with respect to the O-D stretching band, are presented in Fig. 1.

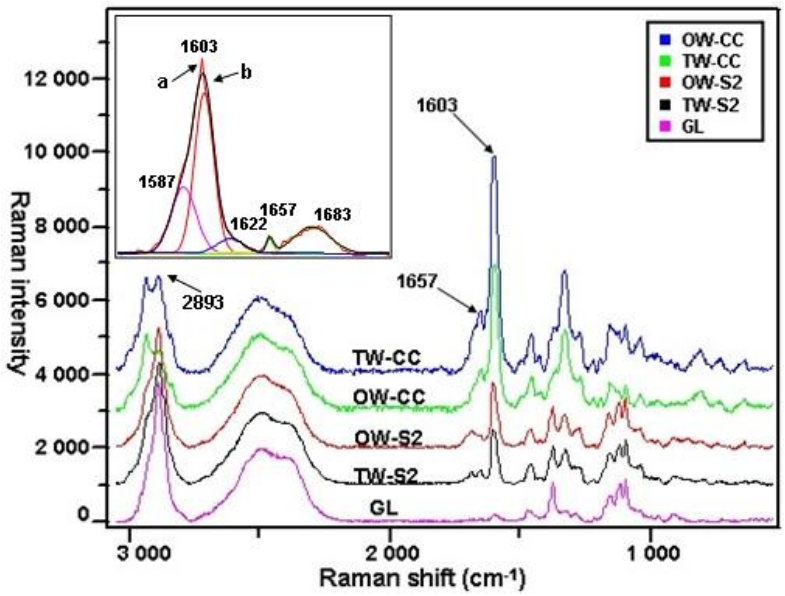

Fig. 1. Average Raman spectra acquired from various layers of OW and TW fiber, 3100-300 cm^{-1}. Inset spectral region showing the deconvolved Gauss-lorenz fits to the spectra, Line a: experimental spectrum; Line b: calculated spectrum from curve-fit data

The Raman bands are attributable primarily to the major wood polymers found in poplar. It is noted that in the region between 1700 and 1500 cm^{-1} the vastly dominant spectral contribution stems from lignin. There are four evident peaks at 1587 cm^{-1}, 1603 cm^{-1}, 1622 cm^{-1}, and 1657 cm^{-1}, which are useful markers of lignin (Agarwal and Ralph 1997). The spectral region from 3000 to 2771 cm^{-1} is assigned to C-H stretching in lignin and carbohydrates. Specifically, the peak at 2893 cm^{-1} is attributed to C-H stretching of cellulose (Wiley and Atalla 1987; Edwards *et al.* 1997).

Morphological Properties of OW and TW Fiber

Chemical images were calculated by integrating over defined bands observed in the wood average spectra. The morphology of the measured fiber cell wall in OW and TW became apparent in the chemical images based on the C-H stretching bands (3000 to 2771 cm^{-1}) in which all cell wall polymers (cellulose, hemicellulose, pectin, and lignin) contribute to the Raman signal. In OW cell corners (CC), compound middle lamella (CML) and middle layer of secondary wall (S2) were easily differentiated (Fig. 2a), while in TW fiber, an additional gelatinous layer (GL) was readily resolved from the S2 and appeared as wavy structures (Fig. 2b). The formation of GL affected the development of S2 (2.2-2.8 μm) in TW, which appeared consistently thinner than that (3.2-4.1 μm) in OW.

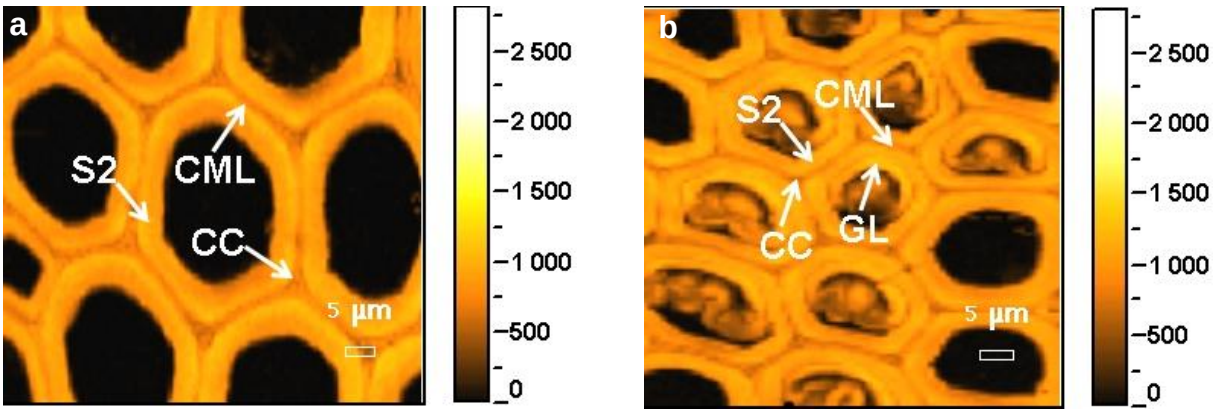

Fig. 2. Raman images calculated by integrating over Raman bands attributed to different functional groups of cell wall polymers. The overall structures of OW (a) and TW (b) fiber, 3000-2771 cm^{-1}. CC, cell corner; CML, compound middle lamella; S2, middle layer of secondary wall; GL, gelatinous layer

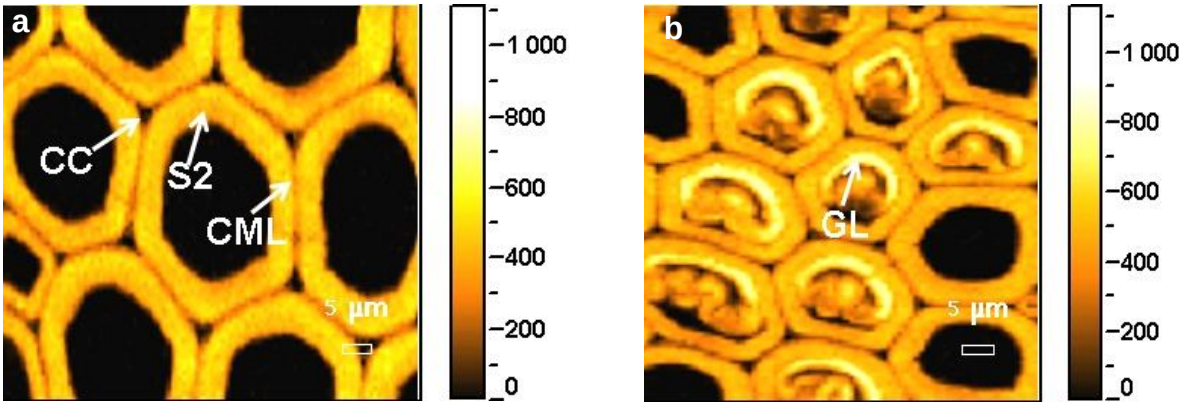

Fig. 3. Raman images calculated by integrating over Raman bands attributed to different functional groups of cell wall polymers. The cellulose distribution in various layers of OW (a) and TW (b) fiber, 2920-2768 cm^{-1}

Compositional Distribution of OW and TW Fiber

Besides the cell wall structures, the distribution of cell components (cellulose and lignin) were also visualized. Cellulose was chosen for Raman imaging analysis because cellulose is the major source of sugar for biofuel production. By integrating over the CH and CH_2 stretching vibrations (2920 to 2768 cm^{-1}), cellulose distribution in the wood cells was visualized. In OW fibers, the highest intensity was found in the fiber S2 and the fewest in the CC as well as the CML (Fig. 3a). By comparison in TW fibers, high cellulose concentration spots were confined mostly to the GL (Fig. 3b). Moreover, it was noted that within the GL, there are regions with lower intensity due to the fact that these areas were up or down the focus plane. This artifact was caused by sample preparation.

Lignin, interwoven with cellulose and hemicelluloses, is one of the primary sources of recalcitrance in biomass conversion. By integrating over the 1603 cm^{-1} band, assigned to the aromatic ring stretching vibration, the distribution of lignin was visualized. In OW fiber, there was strong contrast between morphologically distinct cell wall regions due to different lignin signal intensity (Fig. 4a). The higher lignin signal intensity was observed in CC and was somewhat lower in other regions of the CML. Within the fiber S2, less yet not insubstantial amounts of lignin were observed. By contrast, there were marked differences for the TW fiber (Fig. 4b). While the lignin signal intensity was still higher in the CC, and higher in the CML than in the S2, there was a clear overall reduction of lignin compared to OW fiber, especially in the GL where lignin was significantly depleted.

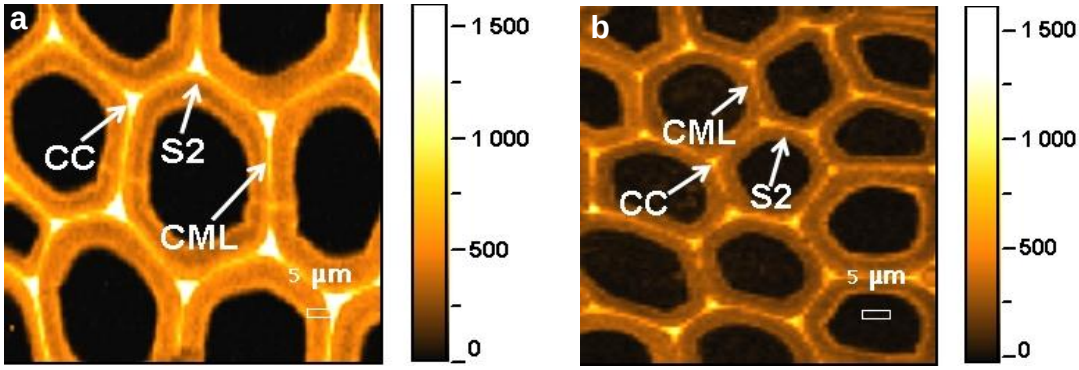

Fig. 4. Raman images calculated by integrating over Raman bands attributed to different functional groups of cell wall polymers. The lignin distribution in various layers of OW (a) and TW (b) fiber, 1620-1590 cm^{-1}

Moreover, as a major component of the plant cell wall matrix, the lignin distribution also has an effect on the porosity of biomass cell wall. The chemical images based on the O-D stretching band (integrating the intensity from 2775 to 2200 cm^{-1}) showed the porous properties of the cell wall regions, especially in the GL. In OW, the highest intensity and thus high D_2O concentration was found in the S2, followed by the CML, and the least in the CC (Fig. 5a). By contrast, TW fiber high intensity was visualized in the GL where the fewest lignin occurred and where there was less lignified S2. The O-D signal, albeit much weaker, was also observed in the CML and in some parts of the CC (Fig. 5b). As a possible explanation, the higher concentration of D_2O in the GL is related to its porosity. As was reported earlier, the TW has much higher porosity, and it is suggested that high porosity is an attribute of the GL itself (Chang *et al.* 2009). In biomass conversion, the porous feature of the GL was in favor of the movement of pretreatment substances employed and increased accessible specific surface area for enzymatic deconstruction.

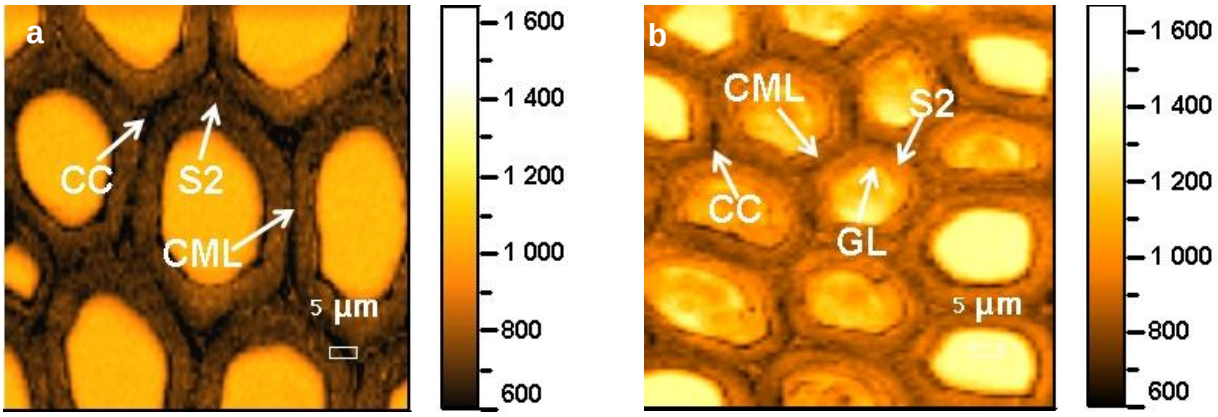

Fig. 5. Raman images showing the D_2O distribution in various layers of OW (a) and TW (b) fiber, 2775 to 2200 cm^{-1}

As the significant precursors of lignin biosynthesis, the distribution of coniferyl alcohol and coniferyl aldehyde (joint abbreviation Lignin-CAA for both structures) in morphologically distinct regions of latewood fiber of the seventh annual ring was also visualized by utilizing the relative band ratios 1657 cm^{-1}/1603 cm^{-1}. The 1657 cm^{-1} band has been assigned to the aromatic ring-conjugated C=C stretching of coniferyl alcohol and C=O stretching of coniferaldehyde (Agarwal and Ralph 2008). As shown in Fig. 6a and 6b, enrichment of Lignin-CAA was observed in the CC and CML regions, where there was the highest lignin concentration, whereas in the fiber S2, where there was the highest content of cellulose, there was an apparent deficiency of the Lignin-CAA concentration. It was evident that both in OW and TW, the Lignin-CAA distribution followed that of lignin. However, in *Picea abies* and *Pinus sylvestris*, the tracheid secondary cell wall contains a higher amount of Lignin-CAA than that of the middle lamella and the primary wall (Hänninen *et al.* 2011). Moreover, earlier studies of phloroglucinol-HCl-stained spruce cell wall by UV-Vis microscopy have shown higher Lignin-CAA group contents in the primary wall and S1 layer (Peng and Westermark 1997). The possible reason for the differences may be that in hardwood lignins, the 1657 cm^{-1} band would have additional contributions from sinapyl alcohol and sinapaldehyde units. As far as what else could be behind the variation in the distribution pattern, the variation could be a reflection of the age of the tree and the position of the sample.

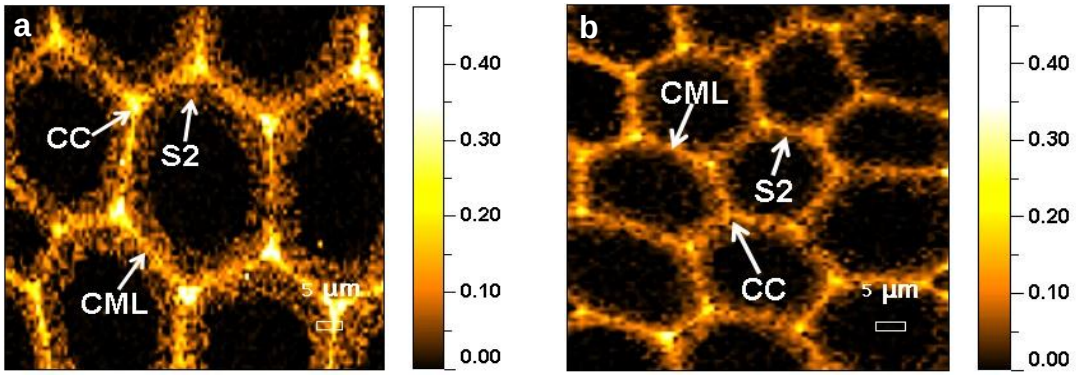

Fig. 6. Raman images calculated by integrating over Raman bands attributed to different functional groups of cell wall polymers. The Lignin-CAA distribution in various layers of OW (a) and TW (b) fiber, $I_{1657\ cm^{-1}}/I_{1603\ cm^{-1}}$

In order to examine variations in the chemical composition of lignin semi-quantitatively, average spectra were extracted from various layers of OW and TW fiber and were normalized at 2500 cm^{-1} (Fig. 1). Compared to OW, TW showed a clear overall decrease in the intensity of the lignin band at 1603 cm^{-1} within various cell wall layers (Table 1). The $I_{1603\ cm^{-1}}/I_{2500\ cm^{-1}}$ ratio was 2.64±0.04 and 0.87±0.02 in OW fiber CC and S2, respectively, while in TW fiber CC and S2, the ratio decreased to 2.03±0.05 and 0.68±0.01, respectively. Considering that the practical lateral resolution in our study (~1 μm) is greater than the thickness of the CML region, we cannot interpret the chemical information from the CML region alone. It may contain a contribution from the adjoining secondary wall. The magnitude of the intensity decrease in all these bands is clearly indicative of an overall reduction in lignin content in TW compared to OW. With respect to the ring conjugated C=C stretching of coniferyl alcohol and C=O stretching of coniferaldehyde, it was noted that the $I_{1657\ cm^{-1}}/I_{2500\ cm^{-1}}$ ratio is higher in TW fiber S2 (0.12±0.01) than in OW fiber S2 (0.08±0.02). Moreover, the detailed analysis of the GL spectra revealed that, at least in some locations, within this layer the lignin related band at 1603 cm^{-1} was present, though not in high enough concentration to be visualized by the imaging approach. The deposition of lignin provides the structural integrity and stiffness of the cell wall (Ralph *et al.* 2007). Thus, a reduction of lignin content in TW fiber can make the cell wall more elastic. As was already suggested by Kubler (1987), the deposition of encrusting lignin between cellulose microfibrils causes transverse expansion of tension wood fibers. Because of the spiral arrangement of the microfibrils, this transverse expansion is associated with longitudinal contraction, just like a wetted rope of twisted natural fibers shortens. Thus, in response to the mechanical stress, the less lignified cell wall was more easily being stretched, which induced the increase of tension stress in the microfibrils in the axial direction.

Table 1. The Relative Intensity of the Lignin Bands within Various Cell Wall Regions

Wood type / Cell wall regions / Band ratio	OW		TW	
	CC	S2	CC	S2
$I_{1657\ cm^{-1}}/I_{2500\ cm^{-1}}$	0.27 (0.01)	0.08 (0.02)	0.25 (0.01)	0.12 (0.01)
$I_{1603\ cm^{-1}}/I_{2500\ cm^{-1}}$	2.64 (0.04)	0.87 (0.02)	2.03 (0.05)	0.68 (0.01)

All values are expressed as the mean (standard deviation) of three individuals

Molecular Deformation Variations in OW and TW Fibers

In response to external physical stimuli such as wind and gravitation, trees regulate the spatial position of their axes by means of active dynamic longitudinal growth stresses in order to restore the trunk to its original vertical position (Scurfield 1973). The mechanism for tree orientation in TW is based on the production of high tensile stress on the upper side of the inclined axis. In many species, the stress level has relations to the presence of the GL (Yoshida *et al.* 2002; Goswami *et al.* 2008; Chang *et al.* 2009; Clair *et al.* 2011). In TW the fibrils in the GL are parallel to the fiber axis, which enable them to deform at approximately the same order of magnitude as the fiber.

When covalent bonds in a fibrous polymer are loaded in tension, their stretching vibrational bands in the infrared or Raman spectrum shift to lower frequency (Wool 1975). At the molecular level, the strain distribution goes via the glucose ring, the C-O-C linkage between these rings (Hinterstoisser *et al.* 2003). In order to investigate the molecular deformation variations in OW and TW fibers, the spectral range from 1750 to 1050 cm^{-1} was extracted (Fig. 7). It was noted that besides changes in the overall Raman intensity, some Raman bands showed obvious changes in band positions (Table 2). The band at 1097.0 cm^{-1} in OW fiber S2 shifted to lower wavenumbers in TW fiber S2 (1094.4 cm^{-1}) and GL (1094.0 cm^{-1}). As was reported earlier, there exists a strong correlation between the shift of the band at 1097 cm^{-1} and the applied strain (r=0.99). Along with increasing strain, the band at 1097 cm^{-1} shifted remarkably to lower wavenumbers (1091 cm^{-1}) (Gierlinger *et al.* 2006). Thus, it was reasonable to assume that TW fiber S2 and GL were in a state of tension during TW formation.

The mechanism at the origin of tensile stress in TW has been explored according to different hypotheses (Clair and Thibaut 2005; Goswami *et al.* 2008; Chang *et al.* 2009; Clair *et al.* 2011). The G-layer swelling hypothesis asserts that the tensional deformation originates in the swelling of the GL and is transmitted to the adjacent secondary layers, where the larger MFAs allow an efficient conversion of lateral stress into axial tensile stress. The cellulose tension hypothesis postulates that tensional stress develops in the G-layer, which then drives shrinkage of the S-layer. Both hypotheses assume that the generation of longitudinal shrinkage in the TW fiber S2 is induced by the GL. The negative band shift of TW fiber S2 and GL in our experiment revealed that after the fibers were transversally cut, the TW fiber S2 and GL still kept the tensional deformation. The tensional deformation of the TW fiber S2 was due to its being in a state of tension during the TW formation. Thus, it can be deduced that both the S2 and GL contribute to the generation of tension strength in the TW fiber simultaneously.

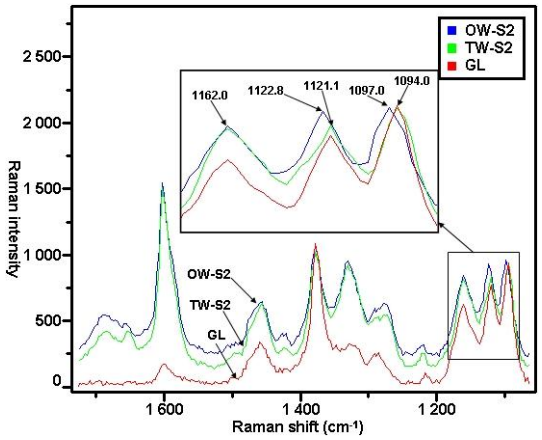

Fig. 7. Average Raman spectra acquired from OW-S2, TW-S2 and GL showing the bandshift of the C-O-C

Table 2. Band Shift of TW-S2 and GL in TW Fiber Relative to Wavenumbers of OW-S2

Wavenumbers (cm^{-1})	Band shift (cm^{-1})	
	TW-S2	GL
1097	2.6 (0.3)	3.0 (0.3)
1123	1.7 (0.4)	1.9 (0.2)
1162	0.4 (0.3)	0.3 (0.2)

All values are expressed as the mean (standard deviation) of three individuals

CONCLUSIONS

1. Label-free *in situ* Raman microspectroscopy combines chemical sensitivity with spatial resolution, making it possible to visualize the topochemical and micromechanical variations between OW and TW. Enrichment of Lignin-CAA was visualized in the CC and CML regions where there was the highest lignin concentration. In fiber S2, which had the highest content of cellulose, there was apparent deficiency in the Lignin-CAA concentration.
3. Considering the reduced lignin content in TW fiber S2 and higher porosity in the GL, TW may be considered as a desirable lignocellulosic biomass with reduced recalcitrance towards enzymatic hydrolysis.
4. Cellulose fibrils in TW fiber S2 and GL became stretched during the TW formation and still remained under tension and contributed to tensile strength even after the stress was released.

ACKNOWLEDGMENTS

This work was supported by the Grants from Natural National Science Foundation of China (31225005 and 31070526), National Science and Technology Program of the Twelfth Five-Year Plan Period (2012BAD32B06) and Doctoral Program of Higher Education of China (20100014110005).

REFERENCES CITED

Agarwal, U. P. and Atalla, R. H. (1986). "In-situ Raman microprobe studies of plant cell walls: Macromolecular organization and compositional variability in the secondary wall of *Picea mariana* (Mill.) B.S.P.," *Planta* 16(3), 325-332.

Agarwal, U. P., and Ralph, S. A. (1997). "FT-Raman spectroscopy of wood: Identifying contributions of lignin and carbohydrate polymers in the spectrum of black spruce (*Picea mariana*)," *Appl. Spectrosc.* 51(11), 1648-1655.

Agarwal, U. P., and Ralph, S. A. (2008). "Determination of ethylenic residues in wood and TMP of spruce by FT-Raman spectroscopy," *Holzforschung* 62(6), 667-675.

Batchelder, D. N., and Bloor, D. (1979). "Strain dependence of the vibrational modes of a diacetylene crystal," *J. Polym. Sci. Pol. Phys.* 17(4), 569-581.

Bowling, A. J., and Vaughn, K. C. (2008). "Immunocytochemical characterization of tension wood: Gelatinous fibers contain more than just cellulose," *Am. J. Bot.* 95(6), 655-663.

Chang, S. S., Clair, B., Ruelle, J., Beauchêne, J., Di Renzo, F., Quignard, F., Zhao, G. J., Yamamoto, H., and Gril, J. (2009). "Mesoporosity as a new parameter for understanding tension stress generation in trees," *J. Exp. Bot.* 60(11), 3023-3030.

Clair, B., and Thibaut, B. (2005). "Shrinkage of the gelatinous layer of poplar and beech tension wood," *IAWA J.* 22 (2), 121-131.

Clair, B., Alméras, T., Pilate, G., Jullien, D., Sugiyama, J., and Riekel, C. (2011). "Maturation stress generation in poplar tension wood studied by synchrotron radiation microdiffraction," *Plant Physiol*. 155(1), 562-570.

Dadwell, H. E., and Wardrop, A. B. (1955). "The structure and properties of tension wood," *Holzforschung* 9(4), 97-104.

Davies, R. J., Eichhorn, S. J., Riekel, C., and Young, R. J. (2004). "Crystal lattice deformation in single poly(p-phenylene benzobisoxazole) fibres," *Polymer* 45(22), 7693-7704.

Edwards, H. G., Farwell, M. D. W., and Webster, D. (1997). "FT-Raman microscopy of untreated natural plant fibers," *Spectrochim. Acta, Part A* 53(13), 2383-2392.

Evans, C. L., and Xie, X. S. (2008). "Coherent anti-stokes Raman scattering microscopy: Chemical imaging for biology and medicine," *Annu. Rev. Anal. Chem.* 1(1), 883-909.

Foston, M., Hubbell, C. A., Samuel, R., Jung, S., Fan, H., Ding, S. Y., Zeng, Y. N., Jawdy, S., Davis, M., Sykes, R., Gjersing, E., Tuskan, G. A., Kalluri, U., and Ragauskas, A. J. (2011). "Chemical, ultrastructural and supramolecular analysis of tension wood in *Populus tremula x alba* as a model substrate for reduced recalcitrance," *Energ. Environ. Sci.* 4(12), 4962-4971.

Fujita, M., Saiki, H., and Harada, H. (1974). "Electron microscopy of microtubules and cellulose microfibirils in secondary wall formation of poplar tension wood fibers," *Mokuzai Gakkaishi* 20(4), 147-156.

Gierlinger, N., Schwanninger, M., Reinecke, A., and Burgert, I. (2006). "Molecular changes during tensile deformation of single wood fibers followed by Raman microscopy," *Biomacromolecules* 7(7), 2077-2081.

Gierlinger, N., and Schwanninger, M. (2007) "The potential of Raman microscopy and Raman imaging in plant research," *Spectro. Int. J.* 21(2), 69-89.

Gomez, L. D., Steele-King, C. G., and McQueen-Mason, S. J. (2008). "Sustainable liquid biofuels from biomass: the writing's on the walls," *New Phytol.* 178(3), 473-485.

Goswami, L., Dunlop, J. W. C., Jungnikl, K., Eder, M., Gierlinger, N., Coutand, C., Jeronimidis, G., Fratzl, P. and Burgert, I. (2008). "Stress generation in the tension wood of poplar is based on the lateral swelling power of the G-layer," *Plant J.* 56(4), 531-538.

Hänninen, T., Kontturi, E., and Vuorinen, T. (2011). "Distribution of lignin and its coniferyl alcohol and coniferyl aldehyde groups in *Picea abies* and *Pinus sylvestris* as observed by Raman imaging," *Phytochemistry* 72(14-15), 1889-1895.

Himmel, M. E., Ding, S. Y., Johnson, D. K., Adney, W. S., Nimlos, M. R., Brady, J. W., and Foust, T. D. (2007). "Biomass recalcitrance: Engineering plants and enzymes for biofuels production," *Science* 315(5813), 804-807.

Hinterstoisser, B., Akerholm, M., and Salmen, L. (2003). "Load distribution in native cellulose," *Biomacromolecules* 4(5), 1232-1237.

Huntley, S. K., Ellis, D., Gilbert, M., Chapple, C., and Mansfield, S. D. (2003). "Significant increases in pulping efficiency in C4H-F5H-transformed poplars: Improved chemical savings and reduced environmental toxins," *J. Agric. Food Chem.* 51(21), 6178-6183.

Kong, K., and Eichhorn, S. J. (2005). "Crystalline and amorphous deformation of process-controlled cellulose-II fibres," *Polymer* 46(17), 6380-6390.

Kubler, H. (1987). "Growth stresses in trees and related wood properties," *For. Prod. Abstr.* 10(3), 61-119.

Iiyama, K., Tuyet Lam, T. B., and Stone, B. A. (1994). "Covalent cross-links in the cell wall," *Plant physiol.* 104(2), 315-320.

Nishikubo, N., Awano, T., Banasiak, A., Bourquin, B., Ibatullin, F., Funada, R., Brumer, H., Teeri, T. T., Hayashi, T., Sundberg, B., and Mellerowicz, E. J. (2007). "Xyloglucan *endo-transglycosylase* (XET) functions in gelatinous layers of tension wood fibers in poplar-A glimpse into the mechanism of the balancing act of trees," *Plant Cell Physio.* 48(6), 843-855.

Peng, F., and Westermark, U. (1997) "Distribution of conifer alcohol and coniferaldehyde groups in the cell wall of spruce fibres," *Holzforschung* 51(6), 531-536.

Pilate, G., Chabbert, B., Cathala, B., Yoshinaga, A., Leplé, J. C., Laurans, F., Lapierre, C., and Ruel, K. (2004). "Lignification and tension wood," *C. R. Biol.* 327(9-10), 889-901.

Ragauskas, A. J., Williams, C. K., Davison, B. H., Britovsek, G., Cairney, J., Eckert, C. A., Frederick, W. J., Hallett, J. P., Leak, D. J., Liotta, C. L., Mielenz, J. R., Murphy, R., Templer, R., and Tschaplinski, T. (2006). "The path forward for biofuels and biomaterials," *Science* 311(5760), 484-489.

Ralph, J., Brunow, G., and Boerjan, W. (2007). "Lignins," In: *Encyclopedia of Life Sciences*, Wiley, Chichester.

Schmidt, M., Schwartzberg, A. M., Perera, P. N., Weber-Bargioni, A., Carroll, A., Sarkar, P., Bosnega, E., Urban, J. J., Song, J., Balakshin, M. Y., Capanema, E. A., Auer, M., Adams, P. D., Chiang, V. I., and Schuck, P. (2009). "Label-free *in situ* imaging of lignifications in the cell wall flow lignin transgenic *Populus trichocarp*," *Planta* 230(3), 589-597.

Siqueira, G., Milagres, A. M. F., Carvalho, W., Koch, G., and Ferraz, A. (2011). "Topochemical distribution of lignin and hydroxycinnamic acids in sugar-cane cell walls and its correlation with the enzymatic hydrolysis of polysaccharides," *Biotechnol Biofuels* 4(1), 7-16.

Scurfield, G. (1973). "Reaction wood: Its structure and function," *Science* 179(4074), 647-655.

Sturcova, A., Davies, G. R., and Eichhorn, S. J. (2005). "Elastic modulus and stress-transfer properties of tunicate cellulose whiskers," *Biomacromolecules* 6(2), 1055-1061.

Tilman, D., Hill, J., and Lehman, C. (2006). "Carbon-negative biofuels from low-input high-diversity grassland biomass," *Science* 314(5805), 1598-1600.

Wiley, J. H., and Atalla, R. H. (1987). "Band assignment in the Raman spectra of celluloses," *Carbohydr. Res.* 160(15), 113-129.

Wool, R. P. (1975) "Mechanisms of frequency shifting in the infrared spectrum of stressed polymer," *J. Polym. Sci.* 13(9), 1795-1808.

Yamamoto, H. (2004). "Role of the gelatinous layer on the origin of the physical properties of the tension wood," *J. Wood Sci.* 50(3), 197-208.

Yoshida, M., Ohta, H., Yamamoto, H., and Okuyama, T. (2002). "Tensile growth stress and lignin distribution in the cell walls of yellow poplar, *Liriodendron tulipifera* Linn," *Trees* 16(7), 457-464.

Zhang, X. B., Zhang, L. H., and Liu, D. H. (2012). "Biomass recalcitrance. Part I: The chemical compositions and physical structures affecting the enzymatic hydrolysis of lignocellulose," *Biofuel. Bioprod. Bior.* 6(4), 465-482.

Zhou, C., Li, Q., Chiang, V. L., Lucia, L. A., and Griffis, D. P. (2011). "Chemical and spatial differentiation of syringyl and guaiacyl lignins in poplar wood via time-of-flight secondary ion mass spectrometry," *Anal. Chem.* 83(18), 7020-7026.

Article submitted: November 5, 2012; Peer review completed: February 2, 2013; Revised version received and accepted: March 7, 2013; Published: March 13, 2013.